· Article ·
doi: 10.13679/j.advps.2014.4.00246

Advances in Polar Science
December 2014 Vol. 25 No. 4: 246-260

Dominant patterns of winter Arctic surface wind variability

WU Bingyi[1*], John Walsh[2], LIU Jiping[3] & ZHANG Xiangdong[2]

[1] Chinese Academy of Meteorological Sciences, Beijing 100081, China;

[2] International Arctic Research Center, University of Alaska Fairbanks, Fairbanks, USA;

[3] Department of Atmospheric and Environmental Sciences, University at Albany, State University of New York, USA

Received 27 May 2014; accepted 4 November 2014

Abstract Dominant statistical patterns of winter Arctic surface wind (WASW) variability and their impacts on Arctic sea ice motion are investigated using the complex vector empirical orthogonal function (CVEOF) method. The results indicate that the leading CVEOF of Arctic surface wind variability, which accounts for 33% of the covariance, is characterized by two different and alternating spatial patterns (WASWP1 and WASWP2). Both WASWP1 and WASWP2 show strong interannual and decadal variations, superposed on their declining trends over past decades. Atmospheric circulation anomalies associated with WASWP1 and WASWP2 exhibit, respectively, equivalent barotropic and some baroclinic characteristics, differing from the Arctic dipole anomaly and the seesaw structure anomaly between the Barents Sea and the Beaufort Sea. On decadal time scales, the decline trend of WASWP2 can be attributed to persistent warming of sea surface temperature in the Greenland—Barents—Kara seas from autumn to winter, reflecting the effect of the Arctic warming. The second CVEOF, which accounts for 18% of the covariance, also contains two different spatial patterns (WASWP3 and WASWP4). Their time evolutions are significantly correlated with the North Atlantic Oscillation (NAO) index and the central Arctic Pattern, respectively, measured by the leading EOF of winter sea level pressure (SLP) north of 70°N. Thus, winter anomalous surface wind pattern associated with the NAO is not the most important surface wind pattern. WASWP3 and WASWP4 primarily reflect natural variability of winter surface wind and neither exhibits an apparent trend that differs from WASWP1 or WASWP2. These dominant surface wind patterns strongly influence Arctic sea ice motion and sea ice exchange between the western and eastern Arctic. Furthermore, the Fram Strait sea ice volume flux is only significantly correlated with WASWP3. The results demonstrate that surface and geostrophic winds are not interchangeable in terms of describing wind field variability over the Arctic Ocean. The results have important implications for understanding and investigating Arctic sea ice variations: Dominant patterns of Arctic surface wind variability, rather than simply whether there are the Arctic dipole anomaly and the Arctic Oscillation (or NAO), effectively affect the spatial distribution of Arctic sea ice anomalies.

Keywords **Arctic, surface wind pattern, sea ice motion, Arctic dipole anomaly**

Citation: Wu B Y, Walsh J, Liu J P, et al. Dominant patterns of winter Arctic surface wind variability. Adv Polar Sci, 2014, 25: 246-260, doi:10.13679/j.advps.2014.4.00246

1 Introduction

The evolution of the Arctic sea ice and its transport out of the Arctic Basin into the Nordic seas and Barents Sea are strongly dependent on the combined forcing by surface winds and ocean currents. Dickson et al.[1] indicated that local wind forcing played an important role in sea ice export into the Greenland Sea during the 1960s, which was associated with the "Great Salinity Anomaly". Walsh and Chapman[2]

* Corresponding author (email: wby@cams.cma.gov.cn)

showed the importance of large-scale wind anomalies over the central Arctic in generating sea ice anomalies. Häkkinen[3] showed that a large part of the fluctuation in sea ice export out of the Arctic could be explained by regional and large-scale anomalous wind patterns. Proshutinsky and Johnson[4] revealed anticyclonic and cyclonic circulation regimes over the Arctic Basin, where each regime persisted for about five to seven years. For the former case, anticyclonic winds are prevalent in the Arctic Basin and sea ice and the water flow towards Fram Strait are reduced because the strengthened Beaufort Gyre accumulates freshwater and sea ice in the Arctic Basin[4-6]. Consequently, sea ice flux from the Arctic Basin into the Greenland Sea is weaker than normal. During the cyclonic regime, there is greater export of sea ice and freshwater out of the Arctic Basin through the Fram Strait because the weakened Beaufort Gyre releases sea ice and freshwater into the Transpolar Drift Stream, within which it is carried to the North Atlantic. Arfeuille et al.[7] have underscored the importance of sea ice evolution in the Arctic Basin and they suggested that sea ice export through the Fram Strait is not simply dependent on local wind in the Fram Strait region, but that the large export of sea ice is preceded by large anomalies of sea ice volume in the Arctic Basin. They showed that anomalies of sea ice volume are generally formed in the East Siberian Sea, which propagate anticyclonically toward the center of the Arctic Basin, prior to being advected directly to the Fram Strait. Wind-induced divergence results in changes of open water area and sea ice thickness, which strongly affect the air sea heat exchange and surface air temperature. Many previous studies focused on the North Atlantic Oscillation (NAO) and Arctic Oscillation (AO) with regard to the atmospheric forcing regimes of the Arctic sea ice. However, recent studies have demonstrated that the AO index might not be a reliable indicator of the Arctic warming and of variations in the Arctic sea ice and North Atlantic conditions[8-13].

Although many previous studies have investigated the influences of atmospheric forcing on the Arctic sea ice[7, 13-17], a number of important questions remain unclear. (1) What are the dominant statistical patterns of winter mean surface wind variability over the Arctic Ocean and its marginal seas? (2) How are these patterns connected to atmospheric circulation anomalies? (3) How to characterize their time evolution? Wu and Johnson[13] did not investigate these questions, but they did reveal the dominant modes of winter (October to March of the next year) monthly mean sea ice motion variability during the period from 1979 to 1998, which reflect surface wind forcing on sea ice motion. In our previous study, the first two modes of winter monthly mean SLP variability north of 70°N was shown to account for 61% and 13% of the variance, respectively (see Figure 1 of Wu et al.[10]). We indicated that because the Arctic dipole anomaly shows strong meridionality, it becomes an important mechanism for driving both anomalous sea ice export out of the Arctic Basin and cold air outbreaks into the Barents Sea, Nordic seas, and northern Europe. However, the crucial issue remains, i.e., why the second mode of SLP variability (the Arctic dipole anomaly) is more important than the first regarding the effect on winter Arctic sea ice (the ratio of their variance contributions is close to 5:1) (see Wu et al.[10]). The motivation behind this study is to find answers to such questions from a dynamical perspective. Vihma et al.[17] suggested that the speed of Arctic sea ice drift is more strongly related to the Central Arctic Index (CAI, calculated by the SLP difference across the Arctic Ocean along meridians 270°E and 90°E) relative to the Arctic dipole anomaly, further demonstrating the limitations of dominant patterns of SLP variability in affecting sea ice motion. In this study, we focus on winter surface wind variability, averaged for three winter (December—February) months. We show that the leading statistical mode of winter mean surface wind variability over the Arctic Ocean and its marginal seas contains two distinct and alternating modes, both of which exhibit strong interannual and decadal variability superposed on declining trends over past decades. It is found that the declining trend of one mode can be attributed to persistent sea surface temperature (SST) warming in the Greenland—Barents—Kara seas from autumn to winter.

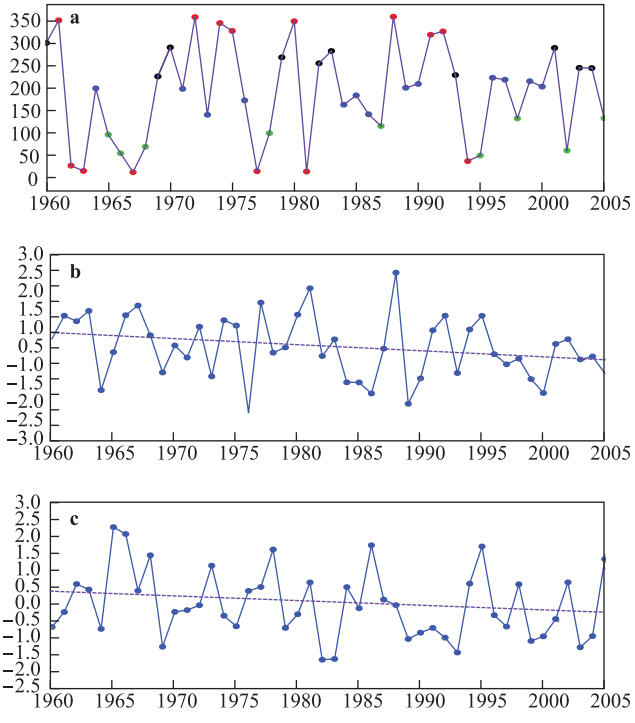

Figure 1 **a**, Time series of the leading phase, and red, green, blue, and black dots denote cases for composite analysis, respectively corresponding to "0°" phase (θ<45° or $\theta \geqslant 315°$), "90°" phase ($135° > \theta \geqslant 45°$), "180°" phase ($225° > \theta \geqslant 135°$), "270°" phase ($315° > \theta \geqslant 225°$); **b**, normalized time series of the real part of the leading complex principal component (solid line) and its linear trend; **c**, same as (b) but for the imaginary part.

2 Data and Methods

The data used in the present study include: (1) monthly mean SLP, surface air temperature (SAT), and surface wind fields (10 m above the ground) for the period 1960—2006 obtained from the NCEP/NCAR re-analysis I; (2) monthly sea ice velocity for the period 1979—2005 obtained from the International Arctic Buoy Programme (IABP, detailed information can be found at http://IABP.apl.washington.edu/); (3) monthly mean Arctic sea ice concentration (SIC) dataset (on a 1° latitude × 1° longitude grid) for the period 1960—2007 obtained from the British Atmospheric Data Centre (BADC, http://badc.nerc.ac.uk/data/hadisst/), (4) monthly mean SST (2-degree) for the period 1960—2007 (http://dss.ucar.edu/datasets/ds277.0/).

Here, we chose 70°—90°N as our study domain, which is consistent with the previous analyses of Johnson et al.[18], Wu et al.[10], and Wu and Johnson[12]. They showed that variations in the Arctic Ocean sea level and SLP were associated with atmospheric patterns poleward of 70ºN. We deliberately did not choose a large domain (from 20° to 90°N), because it would encompass areas beyond the Arctic Basin and its marginal seas where atmospheric forcing would not directly influence sea ice motion. In this study, the complex vector empirical orthogonal function (CVEOF) method is used to extract dominant patterns of winter (DJF) mean Arctic surface wind variability, as in Wu et al.[19]. Additionally, the EOF method is applied to extract dominant patterns of winter SLP variability.

To test the statistical significance in atmospheric circulation and SST anomalies derived from a linear regression, the number of degrees of freedom is taken into account. Additionally, the Monte Carlo technique is applied to examine statistical field significance. For an anomalous field derived from a linear regression, the percentage of grid- points with statistical significance at the 0.05 level is first determined over a domain, and then the same processes are repeated 1 000 times with different series of 46 numbers selected randomly from a normal distribution. If the percentage of grid-points with statistical significance at the 0.05 level is greater than that derived from the 1 000 experiments, the anomalous field is deemed significant.

3 The leading CVEOF of winter Arctic surface wind variability

3.1 Spatial characters

The leading CVEOF of winter mean surface wind variability accounts for 33% of the total variance. We do not show the spatial distribution of the leading eigenvector because it is independent of time (Wu et al.[20]). Figure 1 shows interannual variations of the leading phase, and the real and imaginary parts of the leading complex principal component. To investigate the spatial evolution of the leading CVEOF, we perform composite analyses for the following typical four different leading phase ranges: "0°" phase ($\theta < 45°$ or $\theta \geqslant 315°$), "90°" phase ($135° > \theta \geqslant 45°$), "180°" phase ($225° > \theta \geqslant 135°$), "270°" phase ($315° > \theta \geqslant 225°$). The corresponding chosen cases for the different phase ranges are marked in Figure 1a.

When the leading phase reaches its "0°" phase, an anomalous cyclonic surface wind covers the entire Arctic Basin and its marginal seas. It has a nearly closed center over the eastern Arctic close to the north of the Laptev Sea, and northerly anomalies occupy the Greenland Sea and Barents Sea (Figure 2a). Coherent southwesterly anomalies can be observed over the Kara and Laptev seas. In the Pacific sector, an anomalous anticyclone occupies the northern North Pacific, implying a weakened Aleutian Low. In the North Atlantic sector, southwesterly anomalies cover the North Atlantic, and there is a strong convergence zone that originates from Iceland extending northeastwards to the Kara Sea. When the leading phase is in its "90°" phase, there is a pair of anomalous anticyclonic and cyclonic surface wind fields over the Barents Sea and the Arctic Ocean close to north of the Chukchi Sea, and an anomalous southerly covers the Greenland and the western Barents seas (Figure 2b). Coherent northeasterly anomalies occupy the North Atlantic and most of Europe. In the Pacific sector, an anomalous cyclone covers the Bering Sea, and southerly anomalies would favor additional flow of Pacific water into the Arctic Ocean via the Bering Strait. The anomalous surface wind pattern corresponding to the "180°" phase (Figure 2c) shows the opposite scenario to the "0°" phase (Figure 2a), and the anomalous surface wind pattern corresponding to the "270°" phase (Figure 2d) generally displays an opposite pattern to the "90°" phase (Figure 2b). Thus, one cycle of the spatial evolution of the leading CVEOF is characterized by two alternating and different anomalous surface wind patterns.

3.2 Two different patterns and their impacts on sea ice motion

For any specified spatial point, surface wind variations corresponding to the CVEOF only depend on the real and imaginary parts of the leading complex principal component. Thus, for any spatial point, we can compute its contributions to the surface wind variability through applying a linear regression analysis of winter surface wind fields on the real and imaginary parts. Technically, it is the same as applying a regression analysis of surface wind fields on the winter AO index. It should be pointed out that because the real and imaginary parts of the complex principal components are related to each other, a multiple linear regression analysis is inappropriate for extracting the predominant modes of winter surface wind variability (Wu et al.[19-20]).

Figures 3a and 3b show regression maps of the winter Arctic surface wind fields, on the real (Figure 1b), and imaginary (Figure 1c) parts, respectively. Figure 3a and 3b,

respectively, closely resembles Figure 2a and 2b. Thus, the real and imaginary parts of the leading CVEOF can be used as two indices that separately describe the strength of two different patterns. For clarity in the following discussion, these patterns are referred to as the winter Arctic surface wind pattern 1 (WASWP1) and pattern 2 (WASWP2), respectively. The "0°" and "180°" phase sectors roughly correspond with the real axis, while the "90°" and "270°" phase sectors roughly correspond with the imaginary axis, similar to Wu et al.[19]. Thus, WASWP1 incorporates the "0°" and "180°" phases, while WASWP2 incorporates the "90°" and "270°" phases.

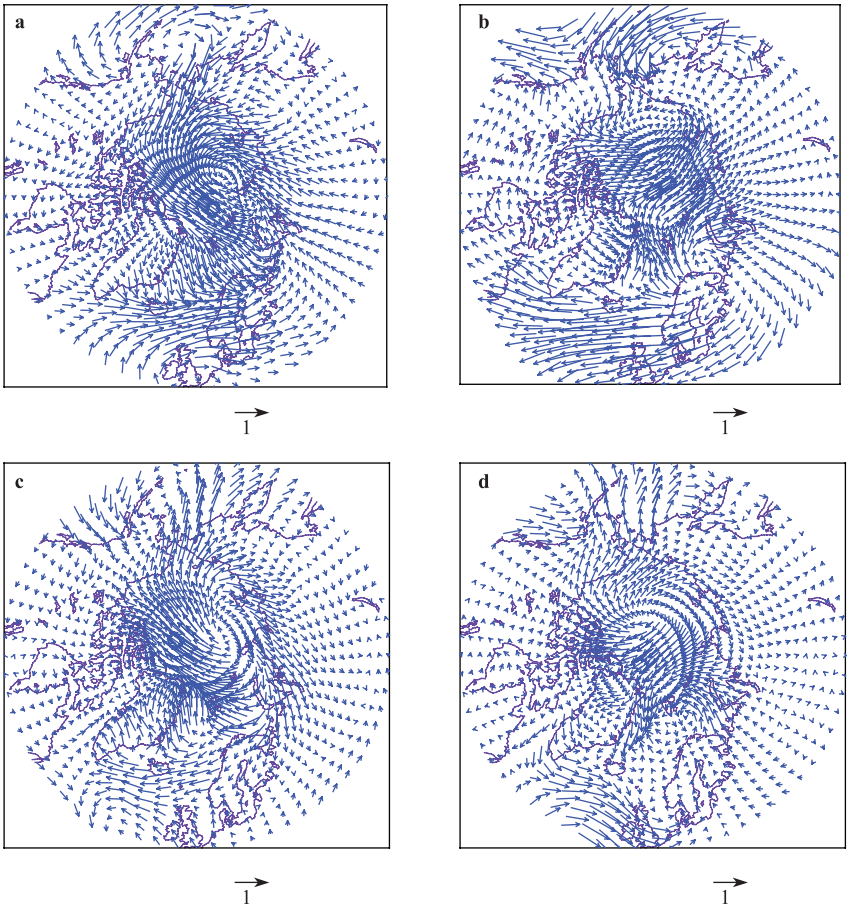

Figure 2 **a**, Composite of winter mean surface wind anomalies for "0°" phase (θ<45° or $\theta\geqslant$315°); **b**—**d**, same as (a) but for "90°" phase (135°>$\theta\geqslant$45°), "180°" phase (225°>$\theta\geqslant$135°), "270°" phase (315°>$\theta\geqslant$225°), respectively (Units: m·s^{-1}).

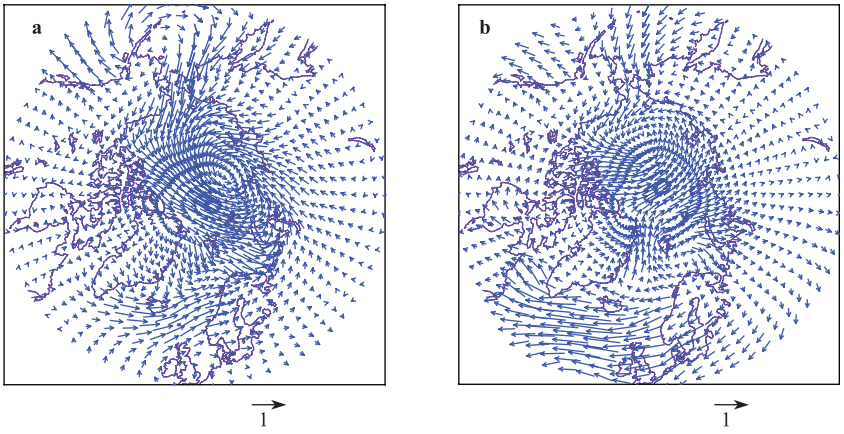

Figure 3 Regression maps of winter mean surface winds on the real part (**a**) and imaginary part (**b**) of the leading complex principal component (Units: m·s^{-1}).

To investigate the temporal structure of the leading CVEOF, a power spectrum analysis is applied to the two patterns. It is found that the spectra of WASWP1 and WASWP2 have dominant peaks quasi-3-year (3.3-year) and 10-year (for WASWP2) periods, respectively, and both are close to the 95% significance level (not shown). Figure 4 shows a 7-year running mean of WASWP1 and WASWP2 and their linear trends. The running mean reflects low-frequency fluctuations that could not be detected in the unsmoothed time series. The maximum (minimum) in WASWP1 occurred in 1964 (1973), 1980 (1987), and 1994 (2002), approximating a 15-year fluctuation (Figure 4a). Positive phases of WASWP1 were frequent before 1982, and then replaced by frequent negative phases. For WASWP2, positive phases were robust before 1979, followed by dominant negative phases subsequently (Figure 4b). Additionally, the quasi-decadal variability is apparent, and the maximum (minimum) can be observed in 1965 (1972), 1975 (1982), 1987 (1990), and 1997 (2001). In fact, both observations and simulations showed the decadal or interdecadal Arctic climate variability[21-28]. Goosse et al.[28] revealed the strong decadal variability of sea ice volume in the Northern Hemisphere with a significant peak at about 15—18 a. Using surface pressure and sea ice concentration, Venegas and Mysak[25] proposed four preferred time scales of variability in the Arctic: 6—7 a, 9—10 a, 16—20 a, and 30—50 a. Köberle and Gerdes[29] suggested that wind forcing significantly contributes to the decadal variability in the Arctic sea ice volume. Thus, decadal variability detected in the two patterns is reasonable and reflects the dominant fluctuations in the coupled air–sea–sea ice system.

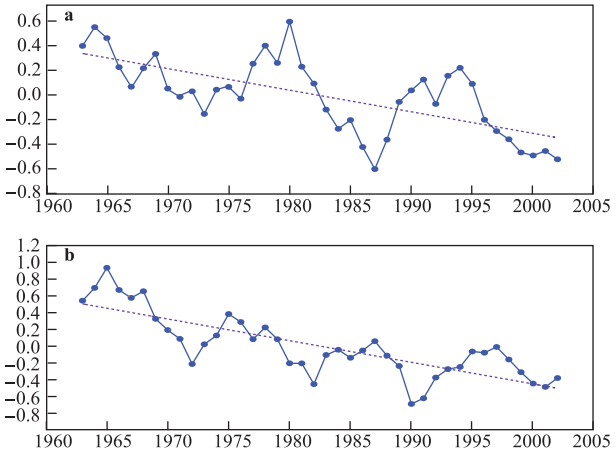

Figure 4 **a**, A 7-year running mean of normalized WASWP1 and its linear trend; **b**, same as (a), but for WASWP2.

Figures 5a and 5b shows regression maps of winter mean sea ice motion, on WASWP1 and WASWP2, respectively. Coherent anomalous cyclonic sea ice motion can be seen in the Arctic Ocean and its marginal seas, with an anomalous center close to the north of the Laptev Sea (Figure 5a). Thus, positive phases of WASWP1 are favorable to above normal transport of sea ice into the Greenland and Barents seas, consistent with the anomalous surface wind forcing shown in Figures 2a and 3a. Sorteberg and Kvingedal[30] suggested that variability in northward-moving cyclones traveling into the Arctic over East Siberia co-varies strongly with sea ice extent in the Barents Sea. They believed that the main mechanism for this is the change in Arctic winds and sea ice advection connected to the cyclones, well consistent with our results presented here (Figures 3a and 5a). Figure 5a indicates that winter sea ice export from the Beaufort Sea into the eastern Arctic is weakened. When WASWP2 reaches its positive phases, a cyclonic anomalous sea ice motion covers the entire Arctic Ocean and its marginal seas, except for the Greenland and Barents seas where ancyclonic anomalous sea ice motion is visible, leading to decreased sea ice transport into the Greenland Sea and increased sea ice export into the Barents Sea (Figure 5b).

The winter sea ice area in the Barents Sea (70.5°—80.5°N and 20.5°—60.5°E) has shown a declining trend in recent decades (Figure 6), and its variation is significantly correlated with both WASWP1 (not shown) and WASWP2 (Figure 6a) (Correlations are 0.32 and 0.41 for 45 winters, exceeding the 0.05 and 0.01 significance levels, respectively). Although the two time series in Figure 6a are broadly similar, individual winters can be radically different. For example, the WASWP2 index was high in the winters of 1986, 1995, and 2005, but the sea ice area was near normal in 1986 and

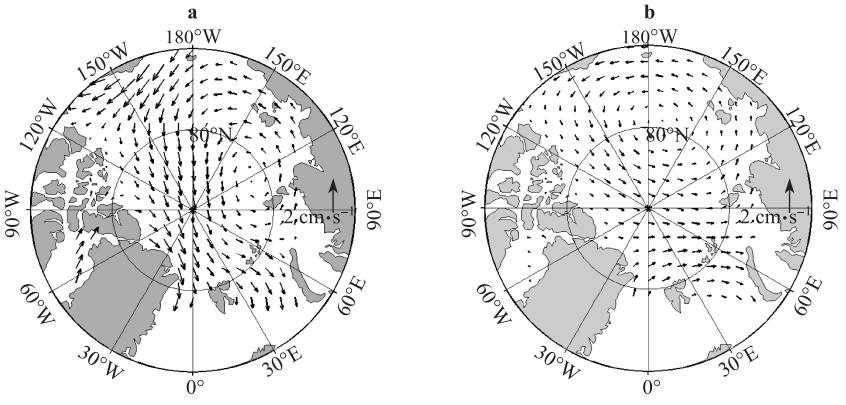

Figure 5 Regression maps of winter mean sea ice motion on WASWP1 (**a**) and WASWP2 (**b**) (Units: cm·s^{-1}).

low in both 1995 and 2005. Thus, a single index such as the WASWP2 index cannot explain fully winter sea ice area anomalies in the Barents Sea, supporting the results of Deser et al.[31] and Maslanik et al.[11]. The North Atlantic warm water is believed to be another important factor influencing winter sea ice area in the Barents Sea (Dickson et al.[32]). Positive sea ice area anomalies can be observed before 1980, then replaced by coherent negative anomalies afterwards, well consistent with the evolution in WASWP2 (Figure 6b).

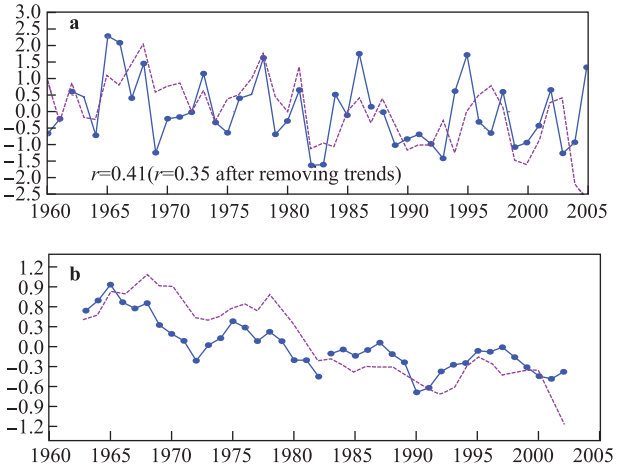

Figure 6 **a**, Normalized time series of WASWP2 (solid line) and winter sea ice area in the Barents Sea (70.5°−80.5°N and 20.5°−60.5°E) (dashed line); **b**, same as (a), but for their 7-year running means. In (a), their correlation is 0.41, exceeding the 0.01 significance level.

3.3 Associations with SLP, 500 hPa height, and surface air temperature

Figure 7 shows regression maps of winter mean SLP and 500 hPa heights on WASWP1 and WASWP2. Figure 7a depicts a tripole structure in winter SLP anomalies, and two positive anomalous centers are located over Western Europe and the Bering Sea with opposite anomalous centers close to the Laptev Sea. It is seen that significant negative SLP anomalies occupy much of the Arctic Ocean and the Siberian marginal seas. Figure 7a shows some similarities to Figure 5c of Wu et al.[10] over the Arctic Ocean and the northern North Pacific, which shows winter (Oct.−Mar.) mean SLP differences associated with the dipole anomaly during the period 1960—2002. Figure 7b resembles Figure 1c of Wu and Johnson[12], which represents monthly mean SLP anomalies derived from a linear regression on the third principal component of EOFs of winter monthly mean SLP north of 70°N during the period 1960−2002. This implies that the leading wind pattern does not show a large similarity to EOF1 of winter SLP variability north of 70°N even though WASWP1 is significantly correlated with the central Arctic pattern (or EOF1) (Table 1). Significant negative SLP anomalies appear between the Beaufort and East Siberian seas, with significant positive SLP anomalies from northern Canada extending eastward to the Kara Sea.

The spatial structure of winter 500 hPa height anomalies associated with WASWP1 (Figure 7c) closely resembles Figure 7a, particularly over the northern North Pacific, Arctic Ocean, and North Atlantic sector, reflecting an equivalent barotropic structure. Whereas 500 hPa height anomalies associated with WASWP2 differ from SLP anomalies, with the positive anomalous center over south of Greenland (Figure 7d) rather than over the Barents Sea (Figure 7b). This implies that atmospheric circulation anomalies related to WASWP2 exhibit some baroclinic characteristics, particularly over the Greenland−Barents seas. It seems that WASWP1 is closely associated with atmospheric circulation anomalies over the northern North Pacific, whereas WASWP2 is more connected to the North Atlantic sector. In fact, there are significant negative correlations between WASWP2 and surface westerly winds over the North Atlantic sector (50°—60°N) (not shown). Figure 7c shows a dipole pattern with opposing anomalous centers over the southeast of the Bering Sea and western North America, closely resembling winter 500 hPa height anomalies associated with the dominant surface wind pattern over the Gulf of Alaska (Figure 8b of Wu and Johnson[33]). Corresponding surface wind anomalies shown in Figure 3a are also similar to Figure 3b of Wu and Johnson[33]. This indicates that WASWP1 is associated with atmospheric circulation anomalies over the northern North Pacific. Additionally, winter atmospheric circulation anomalies associated with WASWP1 and WASWP2 do not reflect the NAO or AO.

Table 1 Correlations

	Central Arctic pattern	Dipole anomaly	Seesaw structure anomaly	NAO	Fram Strait sea ice volume flux
WASWP1	−0.49*	0.77*	−0.13	0.01	0.19
WASWP2	0.18	0.52*	0.71*	−0.49*	−0.22
WASWP3	−0.51*	−0.30	−0.40*	0.54*	0.47*
WASWP4	0.58*	0.19	−0.53*	−0.32	0.06
Central Arctic pattern		0.00	0.00	−0.54*	0.00
Dipole anomaly			0.00	−0.36	0.13
Seesaw structure anomaly				−0.23	−0.40*
NAO					0.29

Notes: *: Significance level at the 0.01;
Central Arctic pattern: EOF1 of SLP variability;
Dipole anomaly: EOF2 of SLP variability;
Seesaw structure anomaly: EOF3 of SLP variability.

In order to explore the relationship between WASWP1/WASWP 2 and the dominant modes of winter SLP variability, we applied the EOF analysis to the winter mean SLP north of 70°N during the period 1960—2006. The first three EOFs, respectively, account for 71%, 11% and 6% of the variance.

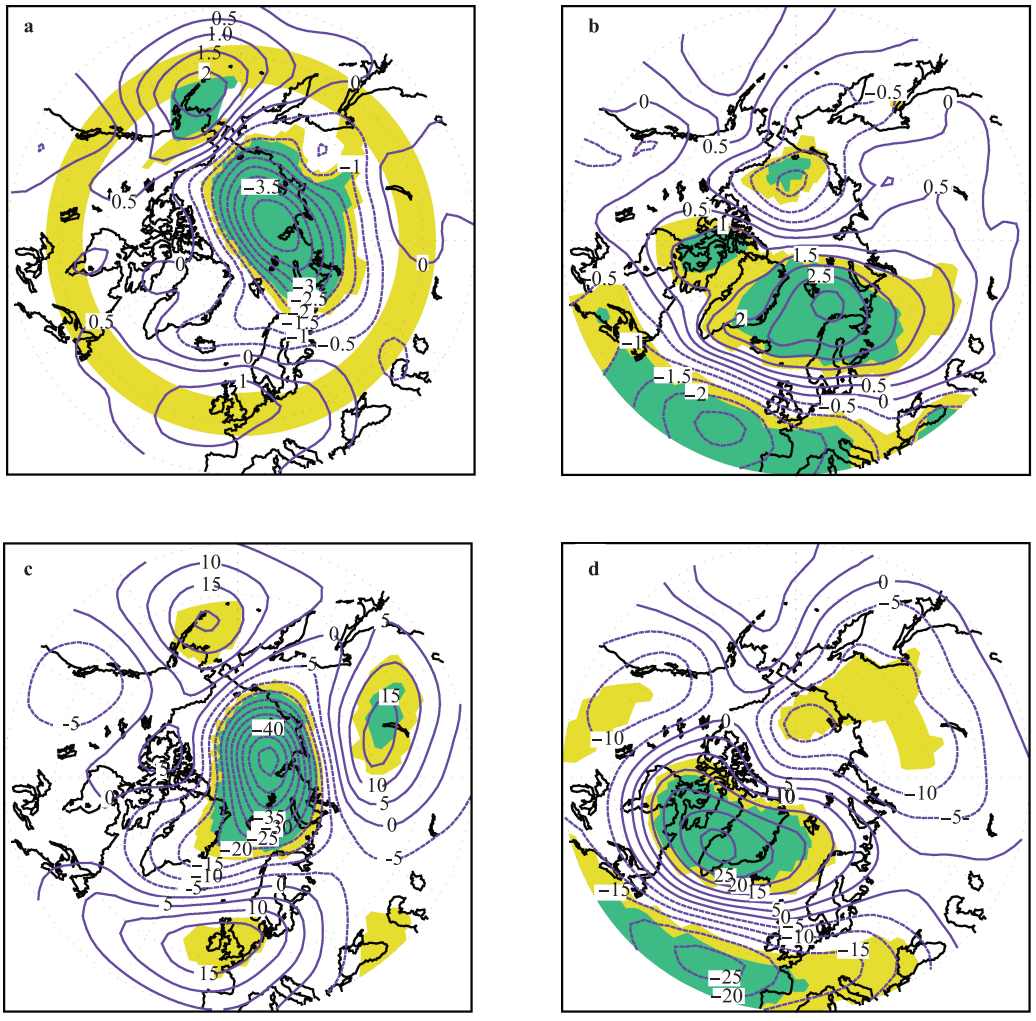

Figure 7 Winter mean SLP anomalies (hPa) derived from a linear regression on WASWP1 (**a**) and WASWP2 (**b**), shaded areas represent SLP anomalies exceeding the 0.05 and 0.01 significance levels, respectively; (**c**) and (**d**) same as (a) and (b), respectively, but for winter 500 hPa height anomalies (gpm).

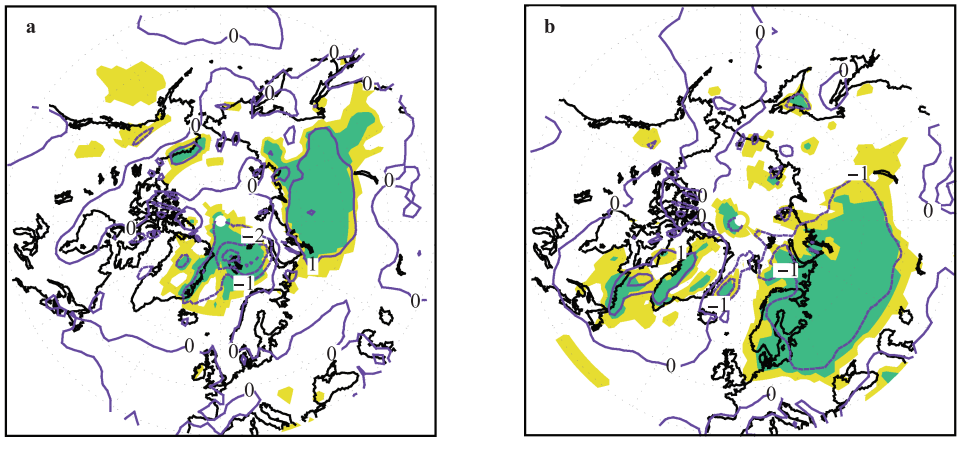

Figure 8 Winter mean SAT anomalies derived from a linear regression, regressed on WASWP1 (**a**) and WASWP2 (**b**), shaded areas are the same as in Figure 7 (Units: °C).

The first three EOFs are well separated from each other and the other EOFs. The first EOF (or the central Arctic pattern) closely resembles the NAO ($r = -0.54$) (Table 1), and the second and third EOFs, respectively, represent the Arctic dipole anomaly and the seesaw structure anomaly between the Beaufort and the Barents seas (Figures 9a, 9b). The correlation between the Arctic dipole anomaly (the seesaw structure anomaly) and WASWP1 (WASWP2) is 0.77 (0.71) (Figure 9c, 9d; Table 1). This implies that the Arctic dipole anomaly approximately reflects WASWP1. This is the reason why the Arctic dipole anomaly plays a greater role in influencing winter Arctic sea ice and its export into the Greenland Sea, relative to the central Arctic pattern or the AO, even though its variance contribution is only 13%. Although both WASWP1 and WASWP2 are closely related to the second and third EOFs of the winter mean SLP variability north of 70°N, their differences in SLP anomalies are visible. For WASWP1 and the Arctic dipole anomaly, large differences emerge from the Bering Sea/Alaska, extending eastward to the Nordic seas (Figures 7a, 9a). For the Arctic dipole anomaly, opposite anomalous centers are respectively located over the Greenland Sea and between the Laptev Sea and the East Siberian Sea (Figure 9a) rather than the Bering Sea and between the Kara and Laptev seas (Figure 7a). Differences between WASWP2 and the seesaw structure anomaly reflect differences in the locations of their anomalous centers (Figures 7b, 9b). Additionally, in Figure 9b, the isoline of 0.5 hPa crosses the Greenland Sea and is parallel to the coastline of Greenland, whereas it is over the Arctic Ocean and perpendicular to the coastline of Greenland in Figure 7b. Further analyses show their differences on interdecadal time scales, particularly in WASWP2 and EOF3, where the rate of decline in WASWP2 is significantly greater than EOF3 (Figures 9e, 9f). More importantly, atmospheric circulation anomalies associated with EOF3 show an equivalent barotropic structure (not shown) rather than some baroclinic

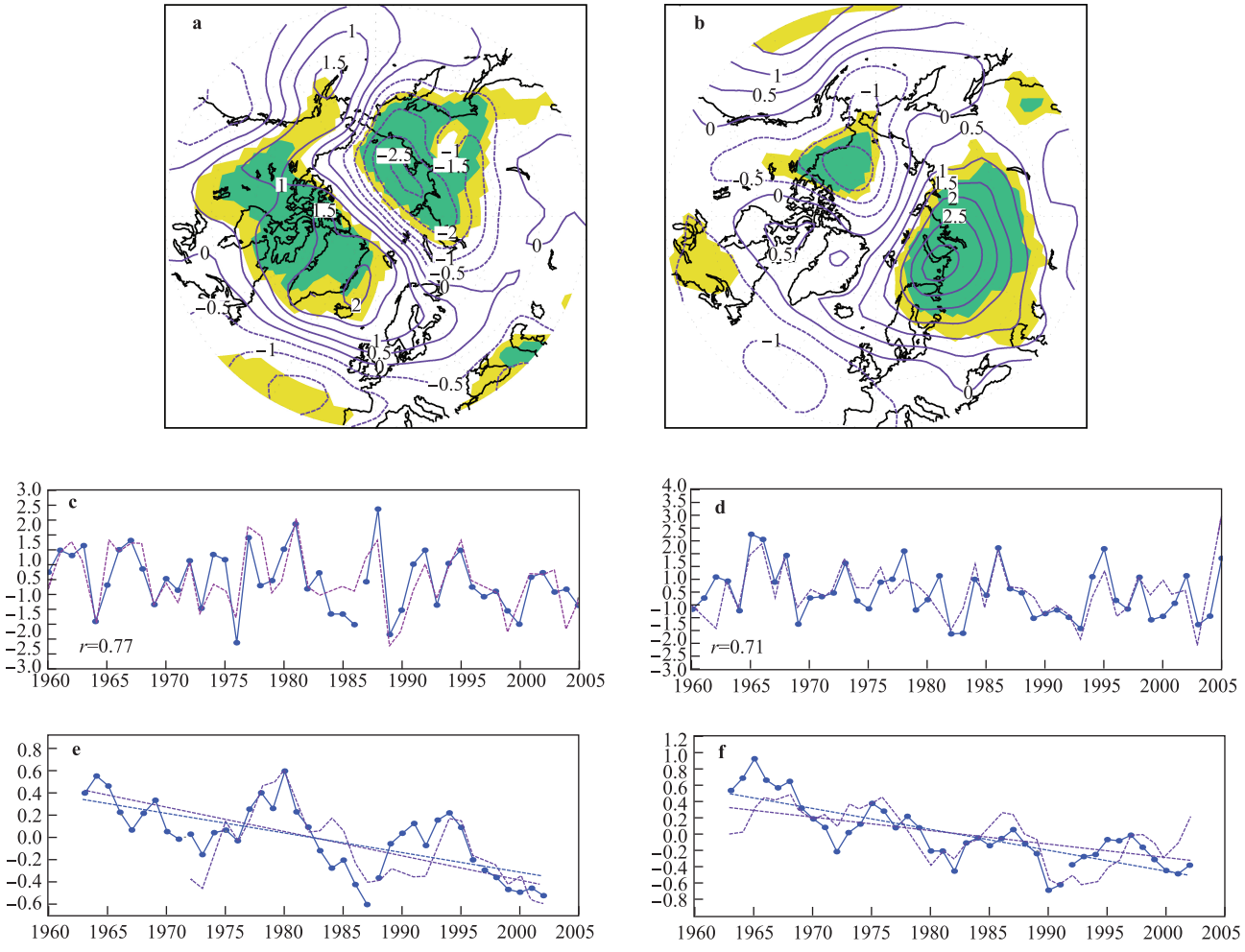

Figure 9 **a**, Regression maps of winter mean SLP, regressed on EOF2 of winter mean SLP variability north of 70°N during winters of 1960/1961 to 2005/2006, the shaded areas are the same as in Figure 7; **b**, same as (a), but for EOF3; **c**, normalized time series of WASWP1 (solid line) and EOF2 (dashed line); their correlation is 0.77; **d**, same as (c), but for WASWP2 (solid line) and EOF3 (dashed line), their correlation is 0.71; **e** and **f** same as (c) and (d), respectively, but for their 7-year running means and linear trends (Units in (a) and (b) are hPa).

characteristics, as shown in Figure 7d. These differences are expectable because the surface wind deviates from the geostrophic wind and the difference between them directly leads to SLP anomalies associated with WASWP1/WASWP2 differing from the dipole anomaly and seesaw structure anomaly between the Beaufort and Barents seas. On the other hand, the surface wind is associated with the geostrophic wind, and this is supported by Thorndike and Colony[34], who found that geostrophic winds account for more than 70% of the variance in daily sea ice motion. Thus, WASWP1 (WASWP2) shows a high positive correlation with the dipole anomaly (the seesaw structure anomaly).

Accompanying surface wind anomalies, SAT also experiences significant variations. When WASWP1 is in its positive phase, a dipole in SAT anomalies is observed over the Greenland and northern Asian continent (Figure 8a). Negative SAT anomalies over the Greenland and Barents seas are dynamically consistent with enhanced cold advection due to the surface wind (Figure 3a). While the positive phase of WASWP2 leads to a decreased SAT over the Barents Sea, northern Europe and western Asian continent (Figure 8b). It is indicated that a positive phase of the winter AO raises SAT over northeastern Asia[35]. Here, we show that a positive phase of WASWP1 (or negative phase of WASWP2) also leads to weak increase of SAT over northeastern Asia. Consequently, different anomalous circulation patterns can promote similar SAT anomalies over northeastern Asia.

4 Second CVEOF of winter Arctic surface wind variability

As two different spatial SLP anomaly patterns corresponding to the leading CVEOF did not resemble the NAO or AO, we further analyze the second CVEOF through a repetition the same process as in Section 3. It is found that the second CVEOF accounts for 18% of the variance and it also contains two different statistical patterns, characterized by their real and imaginary parts of the second complex principal component. We name WASWP3 and WASWP4, respectively. It is seen that the two patterns show strong interannual variability and apparent interdecadal variations (Figures 10a, 10b). In contrast to WASWP1 and WASWP2, there is no trend in both WASWP3 and WASWP4. The power spectrum analysis reveals that both WASWP3 and WASWP4 have no significant period. When WASWP3 is in its positive phase,

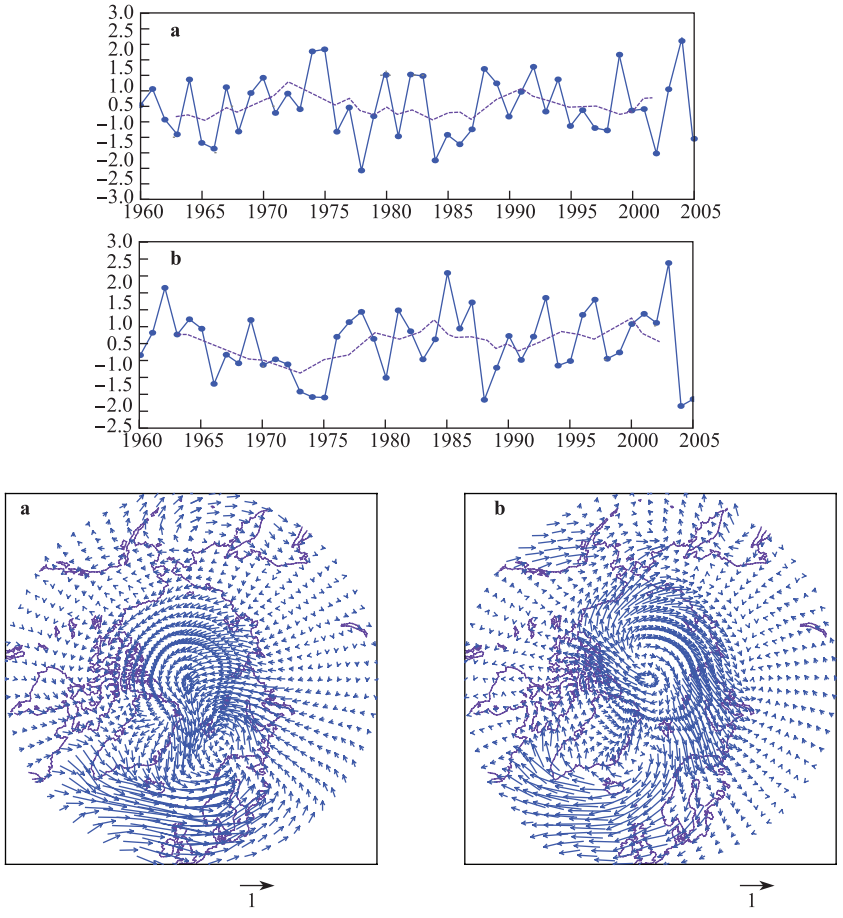

Figure 10 Normalized time series of WASWP3 (**a**) and WASWP4 (**b**), and their 7-year running means (dashed line). Winter mean surface wind anomalies derived from a linear regression on WASWP3 (**c**) and WASWP4 (**d**) (Units: $m \cdot s^{-1}$).

there are coherent cyclonic surface wind anomalies over the entire Arctic Ocean and its marginal seas, with an anomalous center over the western Barents Sea, and anomalies that promote a northerly flow occupy the Fram Strait and the Greenland Sea (Figure 10c). The spatial distribution of corresponding SLP anomalies resembles an extreme positive phase of the NAO (Figure 11a), and there is a significant positive correlation between WASWP3 and the NAO index (r = 0.54, at the 0.01 significance level) (Table 1). As a response to surface wind forcing, sea ice motion anomalies display a weak anomalous cyclone in the Arctic Ocean, except in the East Siberian Sea and Alaskan coastal region where sea ice motion exhibits anticyclonic circulation anomalies (Figure 12a). Anomalous sea ice motion pattern in Figure 12a is well dynamically consistent with SLP anomalies in Figure 11a and it resembles the response of winter sea ice motion to an extreme positive phase of the NAO or AO forcing[14-15]. When WASWP4 reaches its positive phase, an anomalous anticyclone occupies the Arctic Ocean with its center close to the North Pole and coherent northerly anomalies are seen over the Barents Sea (Figure 10d). Over the Greenland Sea, anticyclonic wind anomalies are also visible. Corresponding SLP anomalies show two positive anomalous centers over the Arctic Ocean and the Greenland Sea, respectively (Figure 11b). The anomalous SLP pattern resembles the central Arctic pattern[11]. There is significant positive correlation between WASWP4 and the leading EOF of winter SLP variability north of 70°N (r = 0.58) (The leading EOF of winter SLP variability resembles Figure 1a of Wu et al.[10]) (Table 1). Sea ice motion anomalies show a closed anticyclone in the Arctic Ocean (Figure 12b), similar to the response of sea ice motion to the central Arctic pattern, but with opposite signs[11].

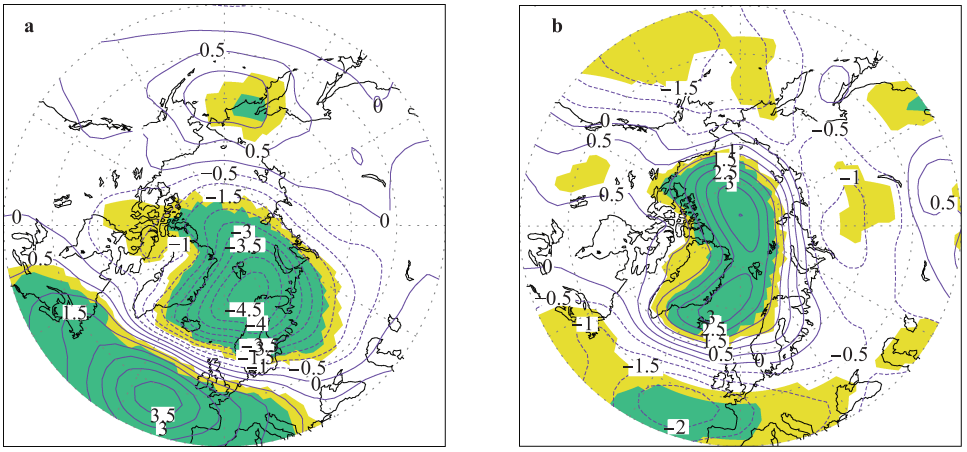

Figure 11 **a**, Winter mean SLP anomalies derived from a linear regression on WASWP3. Shading areas represent SLP anomalies exceeding the 0.05 and 0.01 significance levels, respectively; **b**, same as (a), but for WASWP4 (Units: hPa).

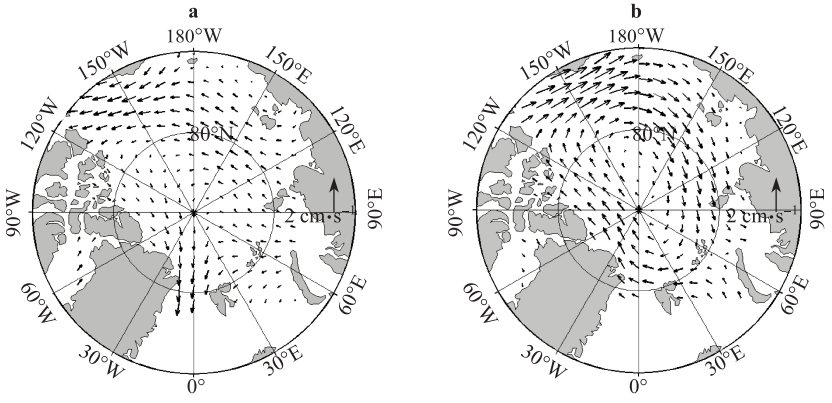

Figure 12 Regression maps of winter mean sea ice motion on WASWP3 (**a**) and WASWP4 (**b**) (Units: cm·s^{-1}).

5 A possible reason for the declining trend in WASWP2

The increasing autumn SST may be a major reason responsible for the weakening of WASWP2, which is illustrated in Figure 13. On interannual time scales, SST warming can be observed in the Greenland—Barents—Kara seas when WASWP2 is in its negative phase (positive SST anomalies exceed 0.1°C, Figure 13a). Similar SST warming also is seen in the same sea region after a linear trend of WASWP2 is removed (not shown). On decadal or longer

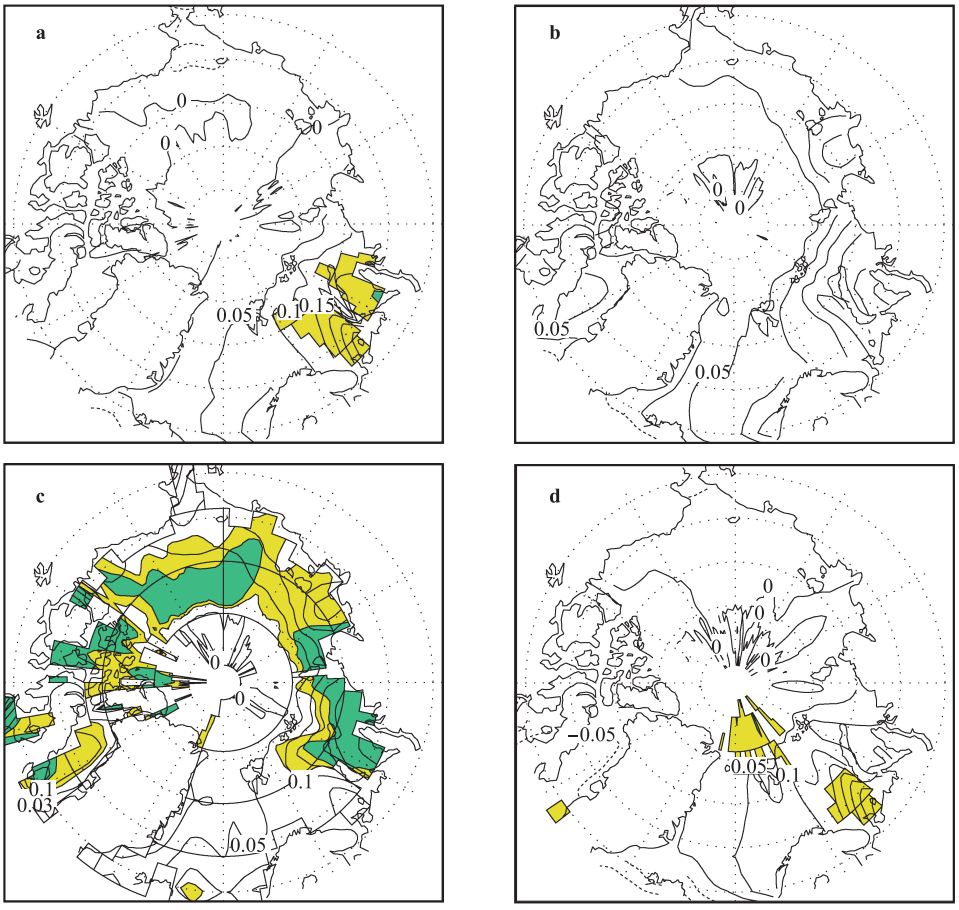

Figure 13 Autumn SST anomalies, derived from a linear regression on WASWP2 (**a**) multiplied by −1.0 during winters of 1960/1961 to 2005/2006; **b**, 7-year running means of WASWP2 multiplied by −1.0; **c**, linear trend of 7-year running means of WASWP2 multiplied by −1.0; **d**, same as (b), but for removing its linear trend. In (a) and (d), shaded areas denote SST anomalies exceeding the 0.05 and 0.01 significance levels, respectively. In (c), shaded areas represent linear trends of autumn SST with the 0.05 and 0.01 significance levels, respectively (Units: °C).

time scales (Figure 4b), WASWP2 related SST warming in the northern Greenland Sea, Barents Sea, Kara Sea and part of the Laptev Sea, but the warming is not statistically significant, and SST anomalies also exceed 0.1°C (Figure 13b). In fact, the time series shown in Figure 4b can be regarded as a linear declining trend plus low frequency fluctuations, and the SST warming in Figure 13b mainly reflects SST anomalies associated with a linear declining trend of WASWP2 (Figure 13c). After removing the linear declining trend in the 7-year running mean time series of WASWP2, SST warming still occurs in the Barents Sea and the Arctic Ocean close to the northern Barents Sea (Figure 13d). The 7-year running means show opposing trends superposed on low frequency fluctuations (their correlation is −0.62, Figure 14a), and their correlation is also significant after removing their linear trends ($r = -0.39$) (not shown). During the winter season, SST warming is also observed from the Barents Sea to the Kara Sea (not shown) and well consistent with the observed winter SAT warming trend over the Barents—Kara seas (see Figure 2b of Zhang et al.[36]). Thus, persistent SST warming in the Greenland—Barents—

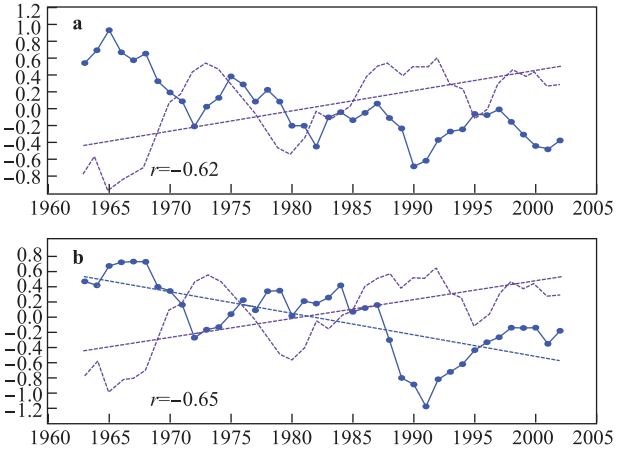

Figure 14 **a**, 7-year running means of normalized WASWP2 (solid line) and autumn regionally-averaged SST (30°—90°E and 70°—80°N) (dashed line) and their linear trends; **b**, 7-year running means of normalized regionally-averaged winter SLP (0°—60°E and 70°—80°N) (solid line) and the autumn SST that is the same as in (a) and their linear trends.

Kara seas favors a decrease in winter SLP over the Nordic and Barents seas, leading to the weakening of WASWP2. The following evidence supports this speculation, as shown Figure 14b. Winter mean SLP in the Greenland-Barents seas (0°—60°E and 70°—80°N) exhibits a declining trend with the 0.01 significance level, and the correlation between the autumn averaged SST and SLP is −0.65 (Figure 14b). After removing the two distinct trends, the correlation becomes −0.48, at the 0.01 significance level. However, on interannual time scales, the winter regionally averaged SLP does not show a significant correlation with autumn SST during the period from 1960 to 2005 (r=−0.24).

6 Impacts on the Fram Strait sea ice flux

Following the procedure of Vinje[37], we use monthly mean SLP (80°N, 10°W and 72.5°N, 20°E) to calculate the approximate wind-induced sea ice volume flux through the Fram Strait. Table 1 shows that WASWP3 and the EOF3 of winter SLP variability (or the seesaw structure anomaly) are significantly correlated with the Fram Strait sea ice volume flux during the period of 1960—2006 (the correlations are 0.47 and −0.40, respectively, exceeding the 0.01 significance level). By contrast, the correlation between the NAO index and the sea ice flux is 0.29 and at the 0.05 marginally significance level (Table 1). Although SLP anomalies associated with WASWP2 (WASWP3) closely resemble the EOF3 of winter SLP variability (the NAO), their impacts on the Fram Strait sea ice flux are different.

7 Dominant patterns of geostrophic wind variability

What is the leading CVEOF of winter geostrophic wind variability over the Arctic Ocean and its marginal seas, and does it correspond well to the dominant statistical patterns of winter SLP variability? To answer these questions, we extract the leading CVEOF of winter geostrophic wind variability derived from the winter mean SLP. The domain for winter geostrophic wind is 70°—87.5°N, 2.5°—355°E. The leading CVEOF accounts for 27% of the variance, which is smaller than that associated with surface wind variability. When the real part of the leading complex principal component is in its positive phase, the anomalous geostrophic wind pattern shows coherent cyclonic anomalies over the Arctic Ocean and its marginal seas, except the Greenland Sea, where the anomalous geostrophic wind is weak (Figure 15a). Although the corresponding SLP anomalies (Figure 15c) exhibit great similarity to the dipole anomaly (Figure 9a), the anomalous center over Alaska and the Bering Sea is robust. Moreover, the correlation between the real part and the dipole anomaly (WASWP1) is 0.89 (0.78). When the imaginary part of the leading complex principal component reaches its positive phase, the anomalous geostrophic wind pattern displays an anticyclonic anomaly with its center close to the northern Kara Sea, while southerly anomalies are seen over Greenland and the Greenland Sea (Figure 15b). Corresponding winter SLP anomalies closely resemble the central Arctic pattern with its anomalous center over the eastern Arctic (Figure 15d). The correlation between the imaginary part and the NAO index (the leading EOF of winter mean SLP variability) is −0.3 (0.66, at the 0.01 significance level). This indicates that the real and imaginary parts in the leading CVEOF are closely correlated to the first two EOFs of winter mean SLP variability. Consequently, the dominant statistical patterns of winter geostrophic wind variability and those of winter surface wind variability are not interchangeable in terms of describing wind field variability over the Arctic Ocean.

8 Discussions

Although the leading CVEOF accounts for 33% of the variance, no effective method is available to identify accurately identify how much variance can be explained by each pattern (WASWP1 and WASWP2). Similarly, we cannot estimate the variance contributed, respectively, by WASWP3 and WASWP4. This is the limitation of this analysis method. It should be pointed out that the identified trend in WASWP1 is meaningful, because the winter surface wind pattern extracted from the ERA-40 re-analysis data during the period from 1960 to 2001 resembles WASWP1 (their correlation is 0.87), and it also shows a declining trend (not shown). The Arctic sea ice motion is influenced by both surface winds and ocean currents, but the importance of the ocean currents is smaller; therefore, this study did not consider the role of ocean currents in sea ice motion variations.

Monte Carlo simulations indicate that those anomalous fields derived from linear regressions, including SAT, SLP, and geopotential heights at 500 hPa, are statistically significant. Although anomalous autumn SST fields shown in Figures 13a and 13d are not significant, linear trends of autumn SST are significant in most of the Arctic Ocean and its marginal seas (Figure 13c), which favor a linear decline of WASWP2. In contrast to WASWP2, the weakening of WASWP1 cannot be attributed to the direct impact of SST warming, since the SST warming in the Greenland—Barents—Kara seas favors a decrease in winter mean SLP, which would strengthen WASWP1. Thus the weakening trend of WASWP1 might reflect an indirect effect of SST and sea ice in the Greenland—Barents—Kara seas. In the Atlantic sector, there is a negative feedback of sea ice on the atmospheric circulation. The atmospheric response to the reduced sea ice in the Greenland—Barents seas and extended sea ice west of Greenland resembles the negative phase of the AO/NAO[38-39], which may cause the weakening of WASWP1 (see Figure 7a of Alexander et al.[38]).

Certainly, all re-analysis data contain uncertainties, particularly in the Arctic. Using observations from drifting ice station in the central Arctic in April—August 2007, Jakobson et al.[38] investigated the validation of atmospheric re-analyses.

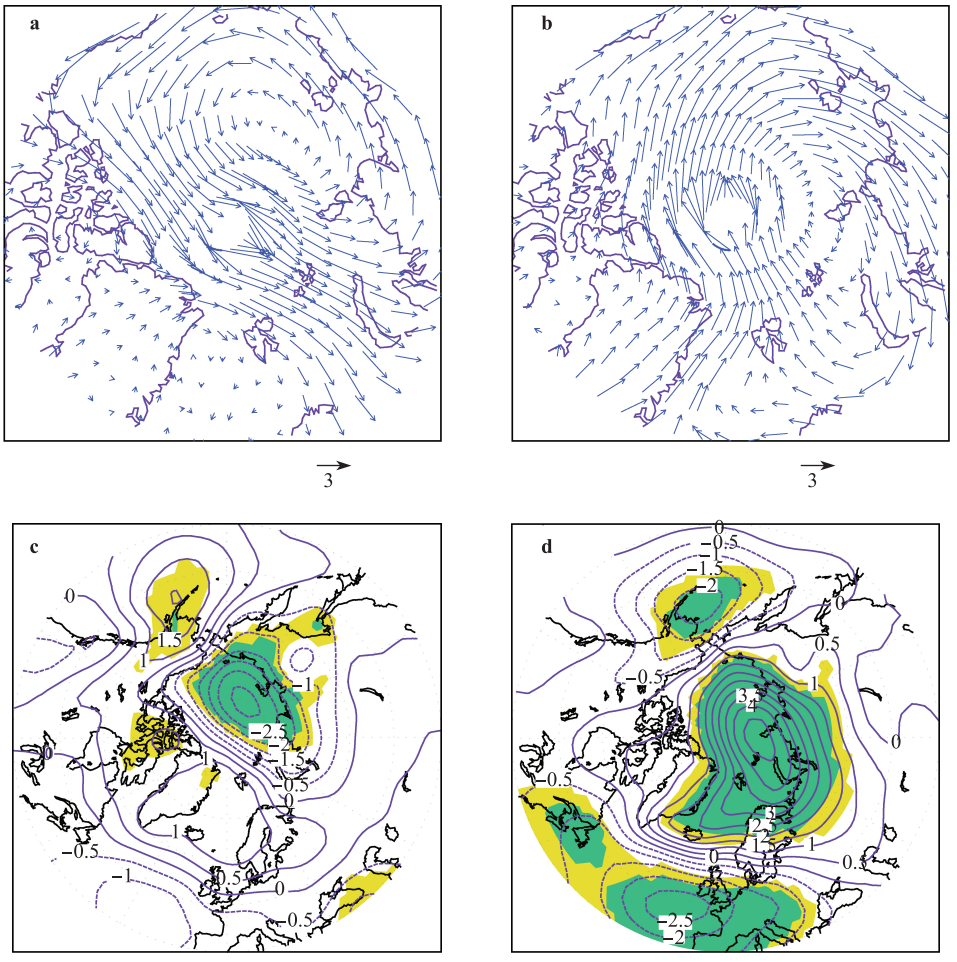

Figure 15 Regression maps of winter mean geostrophic winds on the real part (**a**) and imaginary part (**b**) of the leading complex principal component extracted from the geostrophic wind variability; **c** and **d** same as (a) and (b), respectively, but for SLP anomalies, shaded areas are same as in Figure 7 (Units in (a) and (b) are $m \cdot s^{-1}$; Units in (c) and (d) are hPa).

They indicated that all re-analysis data include large errors, and that ERA-Interim re-analysis data were ranked first. Therefore, it is necessary to investigate further differences in Arctic surface wind patterns derived from different re-analysis data.

9 Summary

Four dominant statistical patterns of winter surface wind variability were identified using the CVEOF method. It was found that the leading CVEOF of winter surface wind variability accounts for 33% of the covariance, and is characterized by two different and alternating patterns (WASWP1 and WASWP2). WASWP1 depicts an anomalous cyclonic (anticyclonic) surface wind over the entire Arctic Basin and its marginal seas, with its center close to the Laptev Sea. WASWP1 shows strong interannual and decadal variations superposed on a linear declining trend over past decades. A positive phase of WASWP1 favors above-normal sea ice export into the Barents Sea and below-normal sea ice export from the Beaufort Sea into the eastern Arctic.

WASWP2 shows a pair of anomalous anticyclonic (cyclonic) and cyclonic (anticyclonic) surface wind fields over the Barents Sea and the Arctic Ocean close to the north of the Chukchi Sea, and an anomalous southerly (northerly) occupies the Greenland Sea and the western Barents Sea. WASWP2 displays strong decadal variation superposed on a linear declining trend over past decades. A positive phase of WASWP2 reduces sea ice exchange between the western and eastern Arctic and enhances sea ice export into the Barents Sea. The persistent negative phase of WASWP2 after 1980 is one of reasons responsible for the decreased winter sea ice area in the Barents Sea. The declining trend of WASWP2 can be attributed to persistent SST warming in the Greenland—Barents—Kara seas from autumn to winter.

Although both WASWP1 and WASWP2 are significantly correlated, respectively, with the dipole anomaly and the seesaw structure anomaly characterized by the second and third EOFs of winter SLP north of 70°N, their corresponding

SLP anomalies obviously differ to some extent from the dipole anomaly and the seesaw structure anomaly over the Arctic Basin and its marginal seas.

The second CVEOF accounts for 18% of the covariance and also contains two different patterns (WASWP3 and WASWP4). Although WASWP3 and WASWP4 also display strong interannual and interdecadal variations there is no apparent trend in both WASWP3 and WASWP4, differing from WASWP1 and WASWP2. WASWP3 shows coherent cyclonic (anticyclonic) surface wind anomalies over the entire Arctic Ocean and its marginal seas, with an anomalous center over the western Barents Sea. Corresponding SLP anomalies resemble the NAO, and there is significant positive correlation between the NAO index and WASWP3 (r = 0.54, at the 0.01 significance level). The Fram Strait sea ice volume flux is only significantly correlated with WASWP3. SLP anomalies associated with WASWP4 reflect the central Arctic pattern characterized by the leading EOF of winter SLP variability north of 70°N. Consequently, winter surface wind anomalies associated with the NAO cannot be considered the most important surface wind pattern over the Arctic Ocean and its marginal seas.

Acknowledgments Authors are grateful to Prof. Timo Vihma and the anonymous reviewers for their support and constructive criticism, which helped significantly to improve this paper. Authors thank the IABP and NCEP/NCAR for providing the sea ice motion data and the re-analysis atmospheric data. This study was jointly supported by the National Key Basic Research Project of China (Grant nos. 2013CBA01804, 2015CB453200), the National Natural Science Foundation of China (Grant nos. 41475080, 41221064), and the Ocean Public Welfare Scientific Research Project of China (Grant no. 201205007).

References

1 Dickson R R, Lamb H H, Malmberg S A, et al. Climatic reversal in northern North Atlantic. Nature, 1975, 256: 479-482.
2 Walsh J E, Chapman W L. Arctic contribution to upper-ocean variability in the North Atlantic. Journal of Climate, 1990, 3: 1462-1473.
3 Häkkinen S. An Arctic source for the great salinity anomaly: a simulation of the Arctic ice-ocean system for 1955-1975. Journal of Geophysical Research, 1993, 98(C9): 16397-16410.
4 Proshutinsky A, Johnson M A. Two circulation regimes of the wind-driven Arctic Ocean. Journal of Geophysical Research, 1997, 102(C6): 12493-12514.
5 Tremblay L B, Mysak L A. On the origin and evolution of sea-ice anomalies in the Beaufort-Chuckchi Sea. Climate Dynamics, 1998, 14: 451-460.
6 Proshutinsky A, Bourke R H, Mclaughlin F A. The role of the Beaufort Gyre in Arctic climate variability: Seasonal to decadal climate scales. Geophysical Research Letters, 2002, 29, 2100, doi: 10.1029/2002GL015847.
7 Arfeuille G, Maysak L A, Tremblay L B. Simulation of the interannual variability of the wind-driven arctic sea-ice cover during 1958-1998. Climate Dynamics, 2000, 16: 107-121.
8 Bengtsson L, Semenov V A, Johannessen O M. The early-century warming in the Arctic—A possible mechanism. Journal of Climate, 2004, 17: 4045-4057.
9 Polyakov E I, Journel A G, Polyakov I V, et al. Changing relationship between the North Atlantic Oscillation and key North Atlantic climate parameters. Geophysical Research Letters, 2006, 33, L03711, doi:10.1029/2005GL024573.
10 Wu B, Wang J, Walsh J. Dipole anomaly in the winter Arctic atmosphere and its association with sea ice motion. Journal of Climate, 2006, 19: 210-225.
11 Maslanik J, Drobot S, Fowler C, et al. On the Arctic climate paradox and the continuing role of atmospheric circulation in affecting sea ice conditions. Geophysical Research Letters, 2007, 34, L03711, doi:10.1029/2006GL028269.
12 Wu B, Johnson M A. A seesaw structure in SLP anomalies between the Beaufort Sea and the Barents Sea. Geophysical Research Letters, 34, 2007, L05811, doi:10.1029/2006GL028333.
13 Wu B, Johnson M A. Distinct modes of winter arctic sea ice motion and their associations with surface wind variability. Advances in Atmospheric Sciences, 2010, 27(2): 211-229.
14 Kwok R. Recent changes in Arctic Ocean sea ice motion associated with the North Atlantic Oscillation. Geophysical Research Letters, 2000, 27: 775-778.
15 Rigor I G, Wallace J M, Colony R L. Response of sea ice to the Arctic Oscillation. Journal of Climate, 2002, 15: 2648-2663.
16 Overland J E, Wang M. The third Arctic climate pattern: 1930s and early 2000s. Geophysical Research Letters, 2005, 32, L23808, doi:10.1029/2005GL024254.
17 Vihma T, Tisler P, Uotila P. Atmospheric forcing on the drift of Arctic sea ice in 1989-2009. Geophysical Research Letters, 39, 2012, L02501, doi:10.1029/2011GL050118.
18 Johnson M A, Proshutinsky A Y, Polyakov I V. Atmospheric patterns forcing two regimes of Arctic ice-ocean circulation: A return to anticyclonic conditions? Geophysical Research Letters, 1999, 26(11): 1621-1624.
19 Wu B, Overland J, D'Arrigo R. Anomalous Arctic surface wind patterns and their impacts on September sea ice minima and trend. Tellus, 2012, 64, 18590, http://dx.doi.org/10.3402/tellusa.v64i0.18590.
20 Wu B, Zhang R, Ding Y, et al. Distinct modes of the East Asian summer monsoon. Journal of Climate, 2008, 21: 1122-1138.
21 Ikeda M. Decadal oscillation of the air-ice-sea system in the northern hemisphere. Atmosphere-Ocean, 1990, 28: 106-139.
22 Mysak L A. Manak D K, Marsden R F. Sea-ice anomalies observed in the Greenland and Labrador Seas during 1901-1984 and their relation to an interdecadal Arctic climate cycle. Climate Dynamics, 1990, 5: 111-133.
23 Walsh J E, Chapman W L, Shy T L. Recent decrease of sea level pressure in the central Arctic. Journal of Climate, 1996, 9: 480-486.
24 Mysak L K, Venegas S A. Decadal climate oscillation in the Arctic: A new feedback loop for atmosphere-ice-ocean interactions. Geophysical Research Letters, 1998, 25: 3607-3610.
25 Venegas S A, Mysak L A. Is there a dominant timescale of natural climate variability in the Arctic? Journal of Climate, 1990, 13: 3412-3434.
26 Polyakov I V, Johnson M A. Arctic decadal and interdecadal variability. Geophysical Research Letters, 2000, 27: 4097-4100.
27 Goosse H, Selten F M, Haarsma R J, et al. A mechanism of decadal variability of the sea-ice volume in the Northern Hemisphere. Climate Dynamics, 2002, 19: 61-83.
28 Goosse H, Holland M M. Mechanisms of decadal Arctic climate variability in the Community Climate System Model, version 2 (CCSM2). Journal of Climate, 2005, 18: 3552-3570.
29 Köberle C, Gerdes R. Mechanisms determining the variability of

Arctic sea ice conditions and export. Journal of Climate, 2003, 16: 2843-2858.

30 Sorteberg A, Kvingedal B. Atmospheric forcing on the Barents Sea winter ice extent. Journal of Climate, 2006, 19: 4772-4784.

31 Deser C, Walsh J E, Timlin M S. Arctic sea ice variability in the context of recent atmospheric circulation trends. Journal of Climate, 2000, 13: 617-633.

32 Dickson R R, Osborn T J, Hurrell J W, et al. The Arctic Ocean response to the North Atlantic Oscillation. Journal of Climate, 2000, 13: 2671-2696.

33 Wu B, Johnson M A. Predominant modes of winter surface wind variability over the Gulf of Alaska. International of Journal of Climate, 2010b, 30: 256-266.

34 Thorndike A S, Colony R. Sea ice motion in response to geostrophic winds. Journal of Geophysical Research, 1982, 87: 5845-5852.

35 Wu B, Wang J. Impacts of winter Arctic Oscillation on Siberian High, the East Asian winter monsoon and sea-ice extent. Advances in Atmospheric Sciences, 2002, 19: 297-320.

36 Zhang X, Sorteberg A, Zhang J, et al. Recent radicall shifts of atmospheric circulations and rapid changes in Arctic climate system. Geophysical Research Letters, 2008, 35, L22701, doi:10.1029/2008GL035607.

37 Vinje T. Fram Strait ice fluxes and atmospheric circulation: 1950-2000. Journal of Climate, 2001, 14: 3508-3517.

38 Alexander M A, Bhatt U S, Walsh J E, et al. The atmospheric response to realistic sea ice anomalies in an AGCM during winter. Journal of Climate, 2004, 17: 890-905.

39 Deser C, Magnusdottir G, Saravanan R, et al. The effects of North Atlantic SST and sea ice anomalies on the winter circulation in CCM3. Part II: Direct and indirect components of the response. Journal of Climate, 2004, 17: 877-889.